

This discussion paper is/has been under review for the journal Atmospheric Measurement Techniques (AMT). Please refer to the corresponding final paper in AMT if available.

# Mapping spectroscopic uncertainties into prospective methane retrieval errors from Sentinel-5 and its precursor

R. Checa-Garcia<sup>1</sup>, J. Landgraf<sup>2</sup>, F. Hase<sup>1</sup>, H. Tran<sup>3</sup>, V. Boudon<sup>4</sup>, F. Alkemade<sup>2</sup>, and A. Butz<sup>1</sup>

<sup>1</sup>IMK-ASF, Karlsruhe Institute of Technology (KIT), Germany

<sup>2</sup>Netherlands Institute for Space Research (SRON), Utrecht, the Netherlands

<sup>3</sup>Laboratoire Interuniversitaire des Systèmes Atmosphériques, Université Paris Est Créteil, Université Paris Diderot, Institut Pierre-Simon Laplace, France

<sup>4</sup>Laboratoire Interdisciplinaire Carnot de Bourgogne, CNRS-Université de Bourgogne, Dijon, France

Received: 2 December 2014 – Accepted: 15 January 2015 – Published: 29 January 2015

Correspondence to: R. Checa-Garcia (ramiro.garcia@kit.edu, r.checagarcia@gmail.com)

Published by Copernicus Publications on behalf of the European Geosciences Union.

AMTD

8, 1333–1363, 2015

Spectroscopic  
uncertainties for CH<sub>4</sub>  
from S5 and S5P

R. Checa-Garcia et al.

Title Page

Abstract

Introduction

Conclusions

References

Tables

Figures

◀

▶

◀

▶

Back

Close

Full Screen / Esc

Printer-friendly Version

Interactive Discussion



## Abstract

Sentinel-5 (S5) and its precursor (S5P) are future European satellite missions aiming at global monitoring of methane ( $\text{CH}_4$ ) column average dry air mole fractions ( $\text{XCH}_4$ ). The spectrometers to be deployed on-board the satellites record spectra of sunlight backscattered from the Earth's surface and atmosphere. In particular, they exploit  $\text{CH}_4$  absorption in the shortwave infrared spectral range around  $1.65\ \mu\text{m}$  (S5 only) and  $2.35\ \mu\text{m}$  (both, S5 and S5P) wavelength. Given an accuracy goal of better than 2 % for  $\text{XCH}_4$  to be delivered on regional scales, assessment and reduction of potential sources of systematic error such as spectroscopic uncertainties is crucial. Here, we investigate how spectroscopic errors propagate into retrieval errors on the global scale. To this end, absorption spectra of a ground-based Fourier Transform Spectrometer (FTS) operating at very high spectral resolution serve as estimate for the quality of the spectroscopic parameters. Feeding the FTS fitting residuals as a perturbation into a global ensemble of simulated S5 and S5P-like spectra at relatively low spectral resolution,  $\text{XCH}_4$  retrieval errors exceed 1 % in large parts of the world and show systematic correlations on regional scales, calling for improved spectroscopic parameters.

## 1 Introduction

The greenhouse gas methane ( $\text{CH}_4$ ) plays a key role in anthropogenically driven climate change (Kirschke et al., 2013). Therefore, monitoring of atmospheric  $\text{CH}_4$  abundances is one of the crucial elements of future Earth observing satellite missions (e.g. Streets et al., 2013). The European Space Agency (ESA) and its national partners have scheduled the Sentinel-5 precursor (S5P), also known as TROPOMI (Veefkind et al., 2012), and the Sentinel-5 (S5) (Ingmann et al., 2012) for launch in 2016 and around 2021, respectively. Both satellites carry spectrometers sensitive to the short-wave infrared (SWIR) spectral range.  $\text{CH}_4$  absorption in sunlight backscattered from the Earth's surface and atmosphere allows for the retrieval of column-average dry air

AMTD

8, 1333–1363, 2015

## Spectroscopic uncertainties for $\text{CH}_4$ from S5 and S5P

R. Checa-Garcia et al.

[Title Page](#)

[Abstract](#)

[Introduction](#)

[Conclusions](#)

[References](#)

[Tables](#)

[Figures](#)

◀

▶

◀

▶

[Back](#)

[Close](#)

[Full Screen / Esc](#)

[Printer-friendly Version](#)

[Interactive Discussion](#)



mole fractions of methane ( $\text{XCH}_4$ ). Thereby, the S5P and S5 strategy builds on the pioneering heritage of the SCanning Imaging Absorption spectrometer for Atmospheric CartographHY (SCIAMACHY) (Bovensmann et al., 1999) and the Greenhouse Gases Observing Satellite (GOSAT) (Kuze et al., 2009) demonstrating that highly accurate satellite remote sensing of  $\text{XCH}_4$  (e.g. Frankenberg et al., 2005; Schneising et al., 2009; Butz et al., 2011; Palmer et al., 2011) can be a valuable tool to gain insight into  $\text{CH}_4$  emissions at the Earth's surface (e.g. Bergamaschi et al., 2007).

Estimating such surface-atmosphere fluxes through inverse modelling, however, poses stringent accuracy requirements on the retrieved  $\text{XCH}_4$ . Regionally or temporally correlated biases as low as 1 % can jeopardize the usefulness of the  $\text{XCH}_4$  satellite records for inverse modelling of surface fluxes (Bergamaschi et al., 2007, 2009). An analogue, potentially even more stringent requirement applies to remote sensing of column-average dry air mole fractions of carbon dioxide ( $\text{XCO}_2$ ) (e.g. Miller et al., 2007; Chevallier et al., 2007; Basu et al., 2013). Therefore, considerable effort is dedicated to estimating and reducing sources of error for  $\text{XCH}_4$  (and  $\text{XCO}_2$ ) retrievals from solar backscatter measurements. Most studies focus on how to avoid or evaluate errors due to lightpath uncertainties in light-scattering atmospheres (e.g. Frankenberg et al., 2005; Oshchepkov et al., 2008; Butz et al., 2009, 2010; Reuter et al., 2010; O'Dell et al., 2012; Buchwitz et al., 2013). In particular, Butz et al. (2012) assess the residual aerosol and cirrus induced  $\text{XCH}_4$  retrieval errors for an S5P-like observer using a global and seasonal ensemble of simulated S5P measurements.

Frankenberg et al. (2008a) demonstrate the detrimental impact of spectroscopic uncertainties on  $\text{XCH}_4$  retrievals and the respective surface flux estimates from SCIAMACHY. They find about 20 % overestimation of the tropical  $\text{CH}_4$  source due to a spurious spectroscopic interference between  $\text{CH}_4$  and water vapor ( $\text{H}_2\text{O}$ ) absorption in the  $1.65 \mu\text{m}$   $\text{CH}_4$  band. In a previous support study for the S5P mission, Galli et al. (2012) degrade high-resolution spectra around  $2.35 \mu\text{m}$  wavelength recorded by ground-based Fourier Transform Spectrometers (FTS) at a mid-latitude and a tropical site to the spectral resolution of the S5P instrument. They conclude on a weak dependence of the

Spectroscopic  
uncertainties for  $\text{CH}_4$   
from S5 and S5P

R. Checa-Garcia et al.

[Title Page](#)

[Abstract](#)

[Introduction](#)

[Conclusions](#)

[References](#)

[Tables](#)

[Figures](#)

◀

▶

◀

▶

[Back](#)

[Close](#)

[Full Screen / Esc](#)

[Printer-friendly Version](#)

[Interactive Discussion](#)



retrieved XCH<sub>4</sub> on spectral resolution and H<sub>2</sub>O content of the atmosphere pointing at relatively little impact of erroneous spectroscopy on XCH<sub>4</sub> retrievals. The spectral fitting residuals in the 2.35 μm band, however, reveal a clearly systematic pattern, which is in particular correlated with H<sub>2</sub>O absorption lines.

5 Here, we aim at mapping spectroscopic errors into XCH<sub>4</sub> retrieval errors for an S5 and S5P-like observer on the global scale in order to assess whether error patterns are significant in magnitude and whether they are correlated among regional spatial and seasonal temporal scales. Such correlations are particularly detrimental for surface flux inversions since they can be readily mistaken for a regional or seasonal flux pattern unlike random noise errors that cancel on the aggregated scales. To this end, the  
10 global ensemble of simulated measurements used previously by Butz et al. (2012) is revisited by replacing the lightpath perturbation through a perturbation due to imperfect spectroscopy. Thereby the spectroscopic perturbation is estimated from fitting residuals to observations of a direct-sun viewing, ground-based Fourier Transform Spectrometer (FTS) operating at very high spectral resolution. Submitting the perturbed satellite  
15 spectra to the retrieval algorithm (which is not aware of the perturbation) allows for assessing the residual XCH<sub>4</sub> forward model error due to imperfect spectroscopy.

This manuscript is organized as follows. Section 2 describes the retrieval algorithm and the general properties of the S5P and S5 trial ensemble. Section 3 strives the  
20 ground-based FTS measurements and introduces the method – and its assumptions – to generate a spectroscopic perturbation among the satellite trial ensemble. Section 4 discusses the spectroscopy induced XCH<sub>4</sub> retrieval errors and Sect. 5 concludes the study.

## 2 Satellite retrieval and trial ensemble

25 Remote sensing of atmospheric parameters in general requires a forward model  $F$  that relates the retrieval parameters chained into the state  $x$  (with  $x_j$  the  $j$ th retrieval

<a href="#">Title Page</a>	
<a href="#">Abstract</a>	<a href="#">Introduction</a>
<a href="#">Conclusions</a>	<a href="#">References</a>
<a href="#">Tables</a>	<a href="#">Figures</a>
<a href="#">◀</a>	<a href="#">▶</a>
<a href="#">◀</a>	<a href="#">▶</a>
<a href="#">Back</a>	<a href="#">Close</a>
<a href="#">Full Screen / Esc</a>	
<a href="#">Printer-friendly Version</a>	
<a href="#">Interactive Discussion</a>	



parameter) from the measurements  $\mathbf{y}$  (with  $y_i$  the  $i$ th spectral element),

$$\mathbf{y} = \mathbf{F}(\mathbf{x}) + \boldsymbol{\epsilon}_y + \boldsymbol{\epsilon}_F. \quad (1)$$

with  $\boldsymbol{\epsilon}_y$  the noise error e.g. due to detector noise and  $\boldsymbol{\epsilon}_F$  the forward model error e.g. due to approximate description of the relevant physics or due to errors of parameters feeding  $\mathbf{F}$ . Here, we intentionally introduce a well-defined spectroscopy-related forward model error  $\boldsymbol{\epsilon}_F$  as described in Sect. 3.

The simulated measurements  $\mathbf{y}$  are spectra of backscattered sunlight in the SWIR spectral range. Thereby, instrument properties are implemented according to the S5 instrument characteristics summarized in Table 1. S5 covers spectral bands from the UV to the SWIR (Ingmann et al., 2012) but here, we focus on the SWIR bands around 1.6  $\mu\text{m}$  (named henceforth SWIR1) and 2.3  $\mu\text{m}$  (named henceforward SWIR3; in the early phase of the mission SWIR2 had been assigned to a channel around 2.0  $\mu\text{m}$  which was dropped later). The finite spectral resolution of the spectrometers is modelled by a Gaussian instrument response function (ISRF) with 0.24 nm width (full width at half maximum (FWHM)). Measurement noise is calculated from a parametric model that considers both, signal-dependent contributions such as photoelectron shot-noise and signal-independent contributions such as dark-current noise. The typical signal to noise ratio (SNR) is in the order of several hundreds for the SWIR bands. Being S5's precursor, S5P features similar instrument characteristics but does not dispose of the SWIR1 channel around 1.6  $\mu\text{m}$ .

The forward model  $\mathbf{F}(\mathbf{x})$  employed here is a variant of the “RemoTeC” algorithm similar to the method used in (Butz et al., 2012). RemoTeC is designed to retrieve XCH<sub>4</sub> (and XCO<sub>2</sub>) for solar backscatter spectra in the SWIR spectral range such as collected by GOSAT, the Orbiting Carbon Observatory (OCO-2), S5P and S5. In its standard setup, the algorithm is able to simulate backscattered radiances in particle loaded atmospheres taking into account lightpath modification by scattering. Here, we focus on the evaluation of spectroscopic errors. Therefore, our study uses a variant of RemoTeC that neglects scattering by aerosols and particles, and the measured spec-

## Spectroscopic uncertainties for CH<sub>4</sub> from S5 and S5P

R. Checa-Garcia et al.

[Title Page](#)

[Abstract](#)

[Introduction](#)

[Conclusions](#)

[References](#)

[Tables](#)

[Figures](#)

◀

▶

◀

▶

[Back](#)

[Close](#)

[Full Screen / Esc](#)

[Printer-friendly Version](#)

[Interactive Discussion](#)



trum depends only on the absorption properties of the target and interfering absorbers described in Table 1. The estimation of those absorption properties relies on HITRAN-2012 spectroscopic parameters (Rothman et al., 2013) assuming a Voigt line-shape. It should be noticed, however, that for line-shape parameters of CH<sub>4</sub> and H<sub>2</sub>O in the SWIR1 and SWIR3 regions, data in HITRAN-2012 are often extrapolated with large uncertainty. Only a small part of the lines was accurately measured or calculated. Neglecting refined line-shape effects (line-mixing, speed dependence and Dicke-narrowing) could also lead to gas retrieval errors (Frankenberg et al., 2008b; Tran et al., 2010; Ghysels et al., 2014). Furthermore, the SWIR1 region in HITRAN-2012 is still not fully characterized, for both line positions and line intensities, compared to other longer wavelength regions (Nikitin et al., 2013; Brown et al., 2013); detailed assignment and lower state energy is not known in many cases affecting line intensity calculations at temperatures other than 296 K. Further experimental and theoretical investigations of this spectral region are presently underway (Tyuterev et al., 2013).

The spectra modelled by RemoTeC are convolved by the satellite's ISRF and noise is added as described above to simulate S5 and S5P-like measurements. Section 3 explains how an extra error due to spectroscopic deficiencies is generated and added to the measurements.

The ensemble of scenes for which we perform retrieval simulations is the same as the one described in detail by Butz et al. (2010) and Butz et al. (2012). While our former studies focus on errors induced by aerosol and cirrus scattering, we neglect such effects here and thus, assume all scenes free of scattering particles. The ensemble covers a day in January, April, July, and October for which we collect atmospheric absorption and surface reflection properties on a ~3° × 3° latitude × longitude grid. Surface albedo in SWIR1 and SWIR3 is assembled from the MODIS land albedo product and a database generated from SCIAMACHY's 2350 nm channel (Schrijver et al., 2009). Meteorological parameters and the abundances of the relevant atmospheric absorbers listed in Table 1 are taken from models (CarbonTracker for CO<sub>2</sub> (Peters et al., 2007),

<a href="#">Title Page</a>	
<a href="#">Abstract</a>	<a href="#">Introduction</a>
<a href="#">Conclusions</a>	<a href="#">References</a>
<a href="#">Tables</a>	<a href="#">Figures</a>
<a href="#">◀</a>	<a href="#">▶</a>
<a href="#">◀</a>	<a href="#">▶</a>
<a href="#">Back</a>	<a href="#">Close</a>
<a href="#">Full Screen / Esc</a>	
<a href="#">Printer-friendly Version</a>	
<a href="#">Interactive Discussion</a>	



TM4 for CH<sub>4</sub> and CO (Meirink et al., 2008), ECHAM5-HAM for H<sub>2</sub>O, temperature and pressure, Stier et al., 2005).

Given the simulated measurements  $\mathbf{y}$ , RemoTeC uses an inverse method based on Philipps–Tikhonov regularization (e.g. Hansen, 1998) to estimate the state vector  $\mathbf{x}$  from Eq. (1). The state vector elements are the 12-layer vertical profiles of CH<sub>4</sub> (and CO<sub>2</sub> partial column concentrations of SWIR1 band is covered), the total column concentrations of the interfering absorbers H<sub>2</sub>O, and CO, and surface reflection parameters (per channel). To find  $\mathbf{x}$ , the inverse method minimizes the cost-function  $\mathcal{J}$  given by

$$10 \quad \mathcal{J}(\mathbf{x}) = \left\| \mathbf{S}_y^{-1/2} (\mathbf{F}(\mathbf{x}) - \mathbf{y}) \right\|^2 + \gamma \|\mathbf{W}(\mathbf{x} - \mathbf{x}_a)\|^2, \quad (2)$$

where  $\mathbf{x}_a$  is the a priori state vector,  $\mathbf{S}_y$  is the diagonal error covariance matrix,  $\mathbf{W}$  is the regularization matrix, and  $\gamma$  is the regularization parameter chosen such that it allows for about 1 degree-of-freedom for the CH<sub>4</sub> (and CO<sub>2</sub>) vertical profiles. The regularization matrix  $\mathbf{W} = \mathbf{L}^T \mathbf{L}$  is assembled from the discrete first-order difference operator  $\mathbf{L}$  for the CH<sub>4</sub> (and CO<sub>2</sub>) vertical profiles and vanishes for all other state vector elements.

Once the state vector solution  $\hat{\mathbf{x}}$  is found it may be written in linear approximation as a combination of the true state  $\mathbf{x}_{\text{true}}$ , the a priori, and the error contributions,

$$\hat{\mathbf{x}} = \mathbf{A}\mathbf{x}_{\text{true}} + (\mathbf{I} - \mathbf{A})\mathbf{x}_a + \mathbf{G}\boldsymbol{\epsilon}_y + \mathbf{G}\boldsymbol{\epsilon}_F \quad (3)$$

where  $\mathbf{A}$  is the averaging kernel and  $\mathbf{G}$  is the contribution or gain matrix (Rodgers, 2000). For our simulations the true state is identical to the a priori ( $\mathbf{x}_{\text{true}} = \mathbf{x}_a$ ), and Eq. (3) reduces to

$$\hat{\mathbf{x}} = \mathbf{x}_{\text{true}} + \mathbf{G}\boldsymbol{\epsilon}_y + \mathbf{G}\boldsymbol{\epsilon}_F \quad (4)$$

Defining an operator  $\mathbf{h}^T$  that selects the CH<sub>4</sub> partial columns from the state vector, adds them up and divides by the total dry air column yields the retrieved dry air mole

[Title Page](#)

[Abstract](#)

[Introduction](#)

[Conclusions](#)

[References](#)

[Tables](#)

[Figures](#)

[◀](#)

[▶](#)

[◀](#)

[▶](#)

[Back](#)

[Close](#)

[Full Screen / Esc](#)

[Printer-friendly Version](#)

[Interactive Discussion](#)



[Title Page](#)[Abstract](#)[Introduction](#)[Conclusions](#)[References](#)[Tables](#)[Figures](#)[|◀](#)[▶|](#)[◀](#)[▶](#)[Back](#)[Close](#)[Full Screen / Esc](#)[Printer-friendly Version](#)[Interactive Discussion](#)

fraction

$$\begin{aligned} X\text{CH}_4 &= \mathbf{h}^T \hat{\mathbf{x}} = \mathbf{h}^T \mathbf{x}_{\text{true}} + \mathbf{h}^T \mathbf{G} \mathbf{e}_y + \mathbf{h}^T \mathbf{G} \mathbf{e}_F \\ &= c_{\text{true}} + \Delta c_y + \Delta c_F. \end{aligned} \quad (5)$$

Since the true state ( $\mathbf{x}_{\text{true}}$  and  $c_{\text{true}}$ ) and the noise realization ( $\mathbf{e}_y$  and  $\Delta c_y$ ) are known, we can evaluate the targeted  $X\text{CH}_4$  forward model error  $\Delta c_F$  by retrieving  $X\text{CH}_4$  from the simulated measurements and subtracting  $c_{\text{true}}$  and  $\Delta c_y$ .

### 3 Generating forward model errors

The first step in generating the spectroscopic forward model error for the satellite retrieval simulations is selecting a set of spectra recorded by the ground-based, direct-sun viewing FTS operated at the Karlsruhe Institute of Technology. The instrument provides wide spectral coverage in all absorption bands relevant here (see Table 1) at very high resolving power  $> 100\,000$ . Such ground-based FTS measurements have been used in previous studies for validating other ground-based instruments (Gisi et al., 2012) and for comparisons to satellite retrievals of  $X\text{CH}_4$  and  $X\text{CO}_2$  (e.g. Guerlet et al., 2013). The FTS-measured atmospheric transmittance spectra are iteratively fitted by a state-of-the-art retrieval method (Hase et al., 2004) fed by the same HITRAN-2012 spectroscopic parameters as the simulated satellite retrievals described in Sect. 2. The adjusted parameters include the vertical profiles of  $\text{CH}_4$  and the relevant interfering species such as  $\text{H}_2\text{O}$ ,  $\text{CO}_2$ ,  $\text{CO}$ , and a background baseline transmittance. Assuming that the residual spectra (difference between the measured and the iteratively adjusted modeled spectrum) are dominated by spectroscopic errors, the residual spectra serve as forward model error perturbation  $\mathbf{e}_F$  for the satellite retrieval simulations.

The methodology we introduce here assumes that the perturbation  $\Delta\tau$  derived from the FTS residuals is dominated by deficiencies of the employed spectroscopic parameters and models. This assumption appears justified by the use state-of-the-art instrumentation and retrieval techniques with a proven performance record. Further, the FTS

residuals represents only a fraction of the actual spectroscopic errors i.e. those cannot be compensated by the free parameters of the FTS fitting routine such as CH<sub>4</sub> and H<sub>2</sub>O abundances. In that sense, the estimated perturbation is an optimistic interpretation of spectroscopic errors.

- 5 For a ground-based, direct-sun viewing observer in a plane parallel atmosphere, the monochromatic atmospheric transmittance  $T_{\text{gb}}$  recorded can be written,

$$T_{\text{gb}}(\tau) = \frac{I_{\text{gb}}(\tau)}{E_S} = \exp\left(-\frac{\tau}{\cos \alpha_{\text{gb}}}\right) \quad (6)$$

- 10 where  $I_{\text{gb}}$  is the observed radiance,  $E_S$  is the solar irradiance at top-of-the-atmosphere,  $\alpha_{\text{gb}}$  is the solar zenith angle of the ground-based sounding, and  $\tau$  is the molecular absorption optical thickness integrated along the zenith direction (i.e. along the vertical). For simplicity, we neglect scattering processes due to molecules and particles. The processing chain of the ground-based FTS measurements provides a best fit  $T_{\text{gb, mod}}$  to the observed transmittance spectra  $T_{\text{gb, true}}$ . The corresponding mismatch

$$\Delta T = T_{\text{gb, true}} - T_{\text{gb, mod}} \quad (7)$$

- 15 is termed the FTS fitting residual to be used for perturbing our simulated satellite retrievals. Figures 1 and 2 show the FTS measured transmittance  $T$  and the fitting residual  $\Delta T$ . Our study uses two different FTS spectra recorded under dry and wet conditions as listed in Table 2. The FTS operates at approximately very high spectral resolution such that the measured residual  $\Delta T$  is approximately equal to the monochromatic residual. Further assuming that the FTS fitting residual is caused by errors in spectroscopic parameters, we can evaluate Eq. (7),

$$\begin{aligned} \Delta T &= \exp\left(-\frac{\tau_{\text{true}}}{\cos \alpha_{\text{gb}}}\right) - \exp\left(-\frac{\tau_{\text{mod}}}{\cos \alpha_{\text{gb}}}\right) \\ &= T_{\text{gb, mod}} \left[ \exp\left(-\frac{\Delta \tau}{\cos \alpha_{\text{gb}}}\right) - 1 \right] \end{aligned} \quad (8)$$

[Title Page](#)

[Abstract](#)

[Introduction](#)

[Conclusions](#)

[References](#)

[Tables](#)

[Figures](#)

◀

▶

◀

▶

[Back](#)

[Close](#)

[Full Screen / Esc](#)

[Printer-friendly Version](#)

[Interactive Discussion](#)



with  $\Delta\tau = \tau_{\text{true}} - \tau_{\text{mod}}$ . Thus, given the FTS residual  $\Delta T$ , the FTS transmittance  $T_{\text{gb, mod}}$ , and the FTS solar zenith angle  $\alpha_{\text{gb}}$ , we can calculate a perturbation  $\Delta\tau$  of the vertical absorption optical thickness

$$\Delta\tau = -\cos\alpha_{\text{gb}} \ln \left( \frac{\Delta T}{T_{\text{gb, mod}}} + 1 \right). \quad (9)$$

- 5 In the next step, the perturbation derived from the ground-based spectra needs translation into a perturbation of the satellite observations. In a non-scattering atmosphere, the reflectance  $R_{\text{sat}}$  observed from a downward-looking space-borne observer is given by

$$R_{\text{sat}}(\tau) = \frac{I_{\text{sat}}(\tau)}{E_S} \quad (10)$$

$$= \frac{A \cos\alpha_{\text{sat}}}{\pi} \exp \left( \frac{\tau}{\cos\alpha_{\text{sat}}} + \frac{\tau}{\cos\theta_{\text{sat}}} \right) \quad (11)$$

where  $I_{\text{sat}}$  is the reflected radiance,  $A$  is the ground albedo,  $\alpha_{\text{sat}}$  is the solar zenith angle and  $\theta_{\text{sat}}$  is the satellite viewing zenith angle (assumed  $\theta_{\text{sat}} = 0^\circ$ , nadir-viewing in our simulation exercise). Replacing the absorption optical thickness  $\tau$  in Eq. (11) by a perturbed optical thickness  $\tau_{\text{per}} = \tau_{\text{mod}} + \Delta\tau$  yields the perturbed satellite measurement.

- 15 Up to here we assume monochromatic light, but in order to introduce the perturbed satellite measurement in the retrieval algorithm we have to take in account the satellite spectral resolution. Therefore, if the satellite retrieval is not aware of this perturbation, the spectroscopic forward model error  $e_F$  amounts to

$$e_F = (R \cdot \mathcal{F}_{\text{sat}})(\tau_{\text{per}}) - (R \cdot \mathcal{F}_{\text{sat}})(\tau). \quad (12)$$

- 20 where  $(R \cdot \mathcal{F}_{\text{sat}})$  represents the convolution of the reflectance by the satellite's ISRF ( $\mathcal{F}_{\text{sat}}$ ). The forward model error  $e_F$  results in the XCH<sub>4</sub> retrieval error  $\Delta c_F$  to be evaluated.

<a href="#">Title Page</a>	
<a href="#">Abstract</a>	<a href="#">Introduction</a>
<a href="#">Conclusions</a>	<a href="#">References</a>
<a href="#">Tables</a>	<a href="#">Figures</a>
<a href="#">◀</a>	<a href="#">▶</a>
<a href="#">◀</a>	<a href="#">▶</a>
<a href="#">Back</a>	<a href="#">Close</a>
<a href="#">Full Screen / Esc</a>	
<a href="#">Printer-friendly Version</a>	
<a href="#">Interactive Discussion</a>	



## Spectroscopic uncertainties for CH<sub>4</sub> from S5 and S5P

R. Checa-Garcia et al.

Figures 1 and 2 reveal variability in  $\Delta\tau$  derived from the two different FTS measurements. Typically, the fitting residuals are larger for the wet than for the dry day. To take into account the dependence on water vapor within the ensemble, the perturbation  $\Delta\tau$  for each simulated scene is estimated by interpolating linearly between the perturbations derived from the two FTS measurements  $\Delta\tau(XH_2O)$  where the interpolation variables is the total column water vapor concentration  $XH_2O$ . The effect of the different viewing geometries is implicitly taken into account by attributing the spectroscopic perturbation to the vertical absorption optical thickness. Figures 3 and 4 shows how  $XH_2O$  and the airmass factor (AMF) vary among our trial ensemble. AMF for the satellite geometry is defined as,

$$AMF_{sat} = \frac{1}{\cos \alpha_{sat}} + \frac{1}{\cos \theta_{sat}} = \frac{1}{\cos \alpha_{sat}} + 1 \quad (13)$$

while the AMF for the ground-based FTS measurements is defined as,

$$AMF_{gb} = \frac{1}{\cos \alpha_{gb}} \quad (14)$$

The satellite soundings are assumed nadir-viewing ( $\theta_{sat} = 0^\circ$ ) with solar zenith angles up to  $\alpha_{sat} = 70^\circ$ , i.e.  $AMF_{sat}$  ranges between 2 and 3.9. The  $XH_2O$  range covered by the FTS measurements is reasonably large (factor 14 between the low and the high value) that we are confident extrapolating to the actual  $XH_2O$  value of the simulated scene. Dependencies of  $\Delta\tau$  on other geophysical variables such as the CH<sub>4</sub> and CO<sub>2</sub> concentrations are neglected, in particular since these concentrations show comparatively little variability in the atmosphere.

Additionally, three processing steps are carried out: first we determine a small spectral shift between the ground-based and the satellite spectra by comparing the FTS transmittance  $T_{gb}$  to simulated satellite soundings at very high instrument resolution. Second, all the FTS measurements are interpolated to the same spectral grid with a resolution of 0.0075 cm<sup>-1</sup>. Third, to avoid spurious large values of  $\Delta\tau$  in the vicinity

[Title Page](#)

[Abstract](#)

[Introduction](#)

[Conclusions](#)

[References](#)

[Tables](#)

[Figures](#)

◀

▶

◀

▶

[Back](#)

[Close](#)

[Full Screen / Esc](#)

[Printer-friendly Version](#)

[Interactive Discussion](#)



of optically thick absorption lines ( $T_{\text{gb}} \rightarrow 0$  in Eq. 9), we adopt a minimum for  $T_{\text{gb}}$  equal to the  $1 - \sigma$  noise level of the FTS spectra.

## 4 Spectroscopy-induced XCH<sub>4</sub> retrieval errors

This section discusses the spectroscopic XCH<sub>4</sub> retrieval errors ( $\Delta c_F$ ) for the three retrieval configurations (SW1, SW3, SW1+3) introduced in Table 1. Thereby, SW3 (covering SWIR3 only) can be considered representative for the S5P setup, SW1+3 (covering SWIR1 and SWIR3), and SW1 (covering SWIR1 only) are possible strategies for S5. Figures 5 through 7 show the residual XCH<sub>4</sub> retrieval errors when introducing the spectroscopic perturbation in our global trial ensemble covering four days in January, April, July, and October. Overall the induced retrieval errors are in the range of a few ten ppb, which is relevant in the view of S5's and S5P's error budget.

The SW1 configuration (Fig. 5) yields an overall overestimation of the true XCH<sub>4</sub>. The retrieval errors are consistently 15–20 ppb larger in the tropics than in mid-to-high-latitudes and the latitudinal pattern of the bias persist over all seasons but is less pronounced for July when the sun is high in the sky. The observed latitudinal correlation appears driven by the dependence of the AMF on latitude and season. Similar patterns have been detected in real XCH<sub>4</sub> retrievals from SCIAMACHY's SWIR1 band though SCIAMACHY exhibited much coarser spectral resolution than the soundings simulated here. Bergamaschi et al. (2009), for example, assume a latitudinal and monthly bias correction for SCIAMACHY XCH<sub>4</sub> to reconcile their source estimates driven by the satellite retrievals and by in situ flask samples. The SW3 configuration (Fig. 6) yields XCH<sub>4</sub> errors that are spatially and temporally variable between roughly –20 and +20 ppb. The error patterns are less correlated with the variation in AMF but tentatively correlate with the variation of total column water vapor XH<sub>2</sub>O. Persistently dry scenes such as the desert areas show very small XCH<sub>4</sub> errors while the seasonally humid mid-latitudes reveal regionally and seasonally variable errors. The tropics, however, show overall small variability of spectroscopy-induced XCH<sub>4</sub> errors. The com-

Title Page

Abstract

Introduction

Conclusions

References

Tables

Figures

◀

▶

◀

▶

Back

Close

Full Screen / Esc

Printer-friendly Version

Interactive Discussion



bined configuration SW1+3 (Fig. 7) yields XCH<sub>4</sub> error patterns that combine the characteristics observed for SW1 and SW3. The latitudinal dependence of residual errors shows up through a general overestimation of XCH<sub>4</sub> in the tropics. In the mid-latitudes a pronounced dependence on the water vapor column overwrites the latitudinal signal.

To illustrate the dependence of the XCH<sub>4</sub> errors on XH<sub>2</sub>O, Fig. 8 shows the correlation between the simulated errors and the water vapor content of the scene. The correlation confirms the above observation that SW1 yields XCH<sub>4</sub> that is less affected by interference from XH<sub>2</sub>O than SW3 but still dry scenes over Siberia and humid ones over the tropics correlate with XCH<sub>4</sub> errors. SW3 retrievals, however, suffer from a strong interference from water vapor which results in underestimation of XCH<sub>4</sub> for very dry scenes, an increasing overestimation for increasingly humid case and then, a decreasing interference from very humid cases. The complicated structure of overlapping CH<sub>4</sub> and H<sub>2</sub>O absorption lines in SWIR3 (Fig. 2) renders such interferences likely. Their detailed mapping on XCH<sub>4</sub> retrieval errors, however, largely depends on the choice of the spectral windows and the spectral resolution of the instrument. The SW1+3 retrievals correlate with water vapor abundances for dry and moderately humid cases but show less dependence on very humid conditions.

These results are consistent with the current status of CH<sub>4</sub> and H<sub>2</sub>O spectroscopy in HITRAN2012. For both SWIR3 and SWIR1, the situation is very challenging for line-shape parameters, namely line-broadening. The SWIR3 region being more intense, and given the large number of CH<sub>4</sub> and H<sub>2</sub>O lines in this region, satellite retrievals from SWIR3 are more affected by air-broadening errors than retrievals from SWIR1. A second reason that may explain the differences between SWIR1 and SWIR3 is that, for SWIR1, there are dedicated studies providing effective Voigt line-shape parameters (Frankenberg et al., 2008b; Nikitin et al., 2010) which lead to the smaller transmittance residuals shown in Fig. 1 compared to Fig. 2.

## Spectroscopic uncertainties for CH<sub>4</sub> from S5 and S5P

R. Checa-Garcia et al.

[Title Page](#)

[Abstract](#)

[Introduction](#)

[Conclusions](#)

[References](#)

[Tables](#)

[Figures](#)

◀

▶

◀

▶

[Back](#)

[Close](#)

[Full Screen / Esc](#)

[Printer-friendly Version](#)

[Interactive Discussion](#)



## 5 Discussion and conclusion

The goals of Sentinel 5 and the Sentinel 5 Precursor concerning XCH<sub>4</sub> retrievals demand a total accuracy better than 2 % (around 30 ppb) in order to allow for successful source and sink estimates on regional and seasonal scales (Bergamaschi et al., 2009).

- 5 Uncertainties due to noise are expected to be in the range of 0.1 % (around 2–3 ppb). Forward model errors are present due to imperfect correction of lightpath modification driven by particle scattering (Butz et al., 2012). The direct consequence is that additional forward model errors e.g. due spectroscopic deficiencies can jeopardize the desired performance. Our assessment estimates such spectroscopy-induced XCH<sub>4</sub> retrieval errors for a global and seasonal ensemble of simulated S5 and S5P-like satellite soundings.
- 10

The key assumption of our approach is that a realistic spectroscopic perturbation can be derived from spectral fitting residuals of a ground-based, direct-sun viewing FTS. This assumption can be criticized in two ways: (1) the FTS fitting residual contains 15 only that part of the spectroscopic errors that cannot be accounted for through the free parameters of the FTS fit i.e. only the part of the spectroscopic errors that are in the null-space (Rodgers, 2000) of the FTS retrieval. (2) The fitting residual contains errors due to other sources than spectroscopy. While flaw (1) would generate overly optimistic XCH<sub>4</sub> errors, flaw (2) would generate overly pessimistic error patterns or an attribution to the wrong error sources. Since the FTS operates at a spectral resolution 20 that allows for fully resolving the atmospheric absorption lines, we expect flaw (1) to be small. Flaw (2) is battled by using an FTS instrument and data reduction methods with demonstrated state-of-the-art performance. Ground-based FTS records such as exploited here, have been used in the past to evaluate spectroscopic parameters (e.g. Frankenberg et al., 2008b; Thompson et al., 2012; Scheepmaker et al., 2013).

25 Translating the ground-based FTS fitting residuals into our satellite sounding ensemble, we consider dependencies on the airmass factor and atmospheric water vapor content but neglect dependencies on other variables such meteorological variables or the

AMTD

8, 1333–1363, 2015

## Spectroscopic uncertainties for CH<sub>4</sub> from S5 and S5P

R. Checa-Garcia et al.

[Title Page](#)

[Abstract](#)

[Introduction](#)

[Conclusions](#)

[References](#)

[Tables](#)

[Figures](#)

◀

▶

◀

▶

[Back](#)

[Close](#)

[Full Screen / Esc](#)

[Printer-friendly Version](#)

[Interactive Discussion](#)



CH<sub>4</sub> abundance itself. This choice renders parameter space treatable and largely follows previous studies that found water vapor interferences (Frankenberg et al., 2008a; Galli et al., 2012) and latitudinal biases (potentially driven by viewing geometry dependencies) (Bergamaschi et al., 2009) the dominating error patterns in XCH<sub>4</sub> from space borne sensors.

Our retrieval simulations indicate that the spectroscopy-induced XCH<sub>4</sub> retrieval errors are significant both, in magnitude and in their spatiotemporal correlation structure. While retrievals from the SWIR1 band (SW1) show a moderate correlation with latitude and water vapor, XCH<sub>4</sub> retrievals from SWIR3 suffer from interferences with water vapor absorption. The observed correlated error patterns generally amount to a few ten ppb which would jeopardize the usefulness of the XCH<sub>4</sub> retrievals for inverse modelling of sources/sinks at the surface.

**Acknowledgements.** This research was funded by the European Space Agency (ESA) through the *Consolidation of S5-SWIR requirements* project: RfQ 3-13741/12/NL/CT/If and by Deutsche Forschungsgemeinschaft (DFG) through the Emmy-Noether programme, grant BU2599/1-1 (RemoteC). The authors would like to thank Manfred Birk and Georg Wagner from DLR for helpful discussions concerning the application of high-resolution atmospheric transmission residuals recorded with ground-based FTIR spectrometers for the estimation of resulting retrieval biases of satellite sensors. We also acknowledge the support by Deutsche Forschungsgemeinschaft and Open Access Publishing Fund of Karlsruhe Institute of Technology.

The service charges for this open access publication have been covered by a Research Centre of the Helmholtz Association.

## References

Basu, S., Guerlet, S., Butz, A., Houweling, S., Hasekamp, O., Aben, I., Krummel, P., Steele, P., Langenfelds, R., Torn, M., Biraud, S., Stephens, B., Andrews, A., and Worthy, D.: Global

## Spectroscopic uncertainties for CH<sub>4</sub> from S5 and S5P

[Title Page](#)

[Abstract](#)

[Introduction](#)

[Conclusions](#)

[References](#)

[Tables](#)

[Figures](#)

◀

▶

◀

▶

[Back](#)

[Close](#)

[Full Screen / Esc](#)

[Printer-friendly Version](#)

[Interactive Discussion](#)



Bergamaschi, P., Frankenberg, C., Meirink, J. F., Krol, M., Dentener, F., Wagner, T., Platt, U., Kaplan, J. O., Körner, S., Heimann, M., Dlugokencky, E. J., and Goede, A.: Satellite chartography of atmospheric methane from SCIAMACHY on board ENVISAT: 2. Evaluation based on inverse model simulations, *J. Geophys. Res.-Atmos.*, 112, D02304, doi:10.1029/2006JD007268, 2007. 1335

Bergamaschi, P., Frankenberg, C., Meirink, J. F., Krol, M., Villani, M. G., Houweling, S., Dentener, F., Dlugokencky, E. J., Miller, J. B., Gatti, L. V., Engel, A., and Levin, I.: Inverse modeling of global and regional  $\text{CH}_4$  emissions using SCIAMACHY satellite retrievals, *J. Geophys. Res.*, 114, 22301, doi:10.1029/2009JD012287, 2009. 1335, 1344, 1346, 1347

Bovensmann, H., Burrows, J., Buchwitz, M., Frerick, J., Noël, S., Rozanov, V., Chance, K., and Goede, A.: SCIAMACHY: mission objectives and measurement modes, *J. Atmos. Sci.*, 56, 127–150, 1999. 1335

Brown, L., Sung, K., Benner, D., Devi, V., Boudon, V., Gabard, T., Wenger, C., Campargue, A., Leshchishina, O., Kassi, S., Mondelain, D., Wang, L., Daumont, L., Régalias, L., Rey, M., Thomas, X., Tyuterev, V. G., Lyulin, O., Nikitin, A., Niederer, H., Albert, S., Bauerecker, S., Quack, M., O'Brien, J., Gordon, I., Rothman, L., Sasada, H., Coustenis, A., Smith Jr., M. T. C., Wang, X.-G., Mantz, A., and Spickler, P.: Methane line parameters in the HITRAN2012 database, *J. Quant. Spectrosc. Ra.*, 130, 201–219, doi:10.1016/j.jqsrt.2013.06.020, 2013. 1338

Buchwitz, M., Reuter, M., Bovensmann, H., Pillai, D., Heymann, J., Schneising, O., Rozanov, V., Krings, T., Burrows, J. P., Boesch, H., Gerbig, C., Meijer, Y., and Löscher, A.: Carbon Monitoring Satellite (CarbonSat): assessment of atmospheric  $\text{CO}_2$  and  $\text{CH}_4$  retrieval errors by error parameterization, *Atmos. Meas. Tech.*, 6, 3477–3500, doi:10.5194/amt-6-3477-2013, 2013. 1335

Butz, A., Bösch, H., Camy-Peyret, C., Chipperfield, M. P., Dorf, M., Kreycy, S., Kritten, L., Prados-Román, C., Schwärzle, J., and Pfeilsticker, K.: Constraints on inorganic gaseous iodine in the tropical upper troposphere and stratosphere inferred from balloon-borne solar occultation observations, *Atmos. Chem. Phys.*, 9, 7229–7242, doi:10.5194/acp-9-7229-2009, 2009. 1335

Butz, A., Hasekamp, O. P., Frankenberg, C., Vidot, J., and Aben, I.:  $\text{CH}_4$  retrievals from space-based solar backscatter measurements: performance evaluation against simulated aerosol

Spectroscopic  
uncertainties for  $\text{CH}_4$   
from S5 and S5P

R. Checa-Garcia et al.

Title Page

Abstract

Introduction

Conclusions

References

Tables

Figures

◀

▶

◀

▶

Back

Close

Full Screen / Esc

Printer-friendly Version

Interactive Discussion



and cirrus loaded scenes, *J. Geophys. Res.*, 115, 24302, doi:10.1029/2010JD014514, 2010.  
1335, 1338

5 Butz, A., Guerlet, S., Hasekamp, O., Schepers, D., Galli, A., Aben, I., Frankenberg, C., Hartmann, J.-M., Tran, H., Kuze, A., Keppel-Aleks, G., Toon, G., Wunch, D., Wennberg, P., Deutscher, N., Griffith, D., Macatangay, R., Messerschmidt, J., Notholt, J., and Warneke, T.: Toward accurate CO<sub>2</sub> and CH<sub>4</sub> observations from GOSAT, *Geophys. Res. Lett.*, 38, L14812, doi:10.1029/2011GL047888, 2011. 1335

10 Butz, A., Galli, A., Hasekamp, O., Landgraf, J., Tol, P., and Aben, I.: TROPOMI aboard Sentinel-5 Precursor: prospective performance of CH<sub>4</sub> retrievals for aerosol and cirrus loaded atmospheres, *Remote Sens. Environ.*, 120, 267–276, doi:10.1016/j.rse.2011.05.030, 2012. 1335, 1336, 1337, 1338, 1346

15 Chevallier, F., Bréon, F.-M., and Rayner, P. J.: Contribution of the Orbiting Carbon Observatory to the estimation of CO<sub>2</sub> sources and sinks: theoretical study in a variational data assimilation framework, *J. Geophys. Res.*, 112, 9307, doi:10.1029/2006JD007375, 2007. 1335

20 Frankenberg, C., Meirink, J. F., van Weele, M., Platt, U., and Wagner, T.: Assessing methane emissions from global space-borne observations, *Science*, 308, 1010–1014, doi:10.1126/science.1106644, 2005. 1335

25 Frankenberg, C., Bergamaschi, P., Butz, A., Houweling, S., Meirink, J. F., Notholt, J., Petersen, A. K., Schrijver, H., Warneke, T., and Aben, I.: Tropical methane emissions: a revised view from SCIAMACHY onboard ENVISAT, *Geophys. Res. Lett.*, 35, L15811, doi:10.1029/2008GL034300, 2008a. 1335, 1347

30 Frankenberg, C., Warneke, T., Butz, A., Aben, I., Hase, F., Spietz, P., and Brown, L. R.: Pressure broadening in the 2v<sub>3</sub> band of methane and its implication on atmospheric retrievals, *Atmos. Chem. Phys.*, 8, 5061–5075, doi:10.5194/acp-8-5061-2008, 2008b. 1338, 1345, 1346

35 Galli, A., Butz, A., Scheepmaker, R. A., Hasekamp, O., Landgraf, J., Tol, P., Wunch, D., Deutscher, N. M., Toon, G. C., Wennberg, P. O., Griffith, D. W. T., and Aben, I.: CH<sub>4</sub>, CO, and H<sub>2</sub>O spectroscopy for the Sentinel-5 Precursor mission: an assessment with the Total Carbon Column Observing Network measurements, *Atmos. Meas. Tech.*, 5, 1387–1398, doi:10.5194/amt-5-1387-2012, 2012. 1335, 1347

40 Ghysels, M., Gomez, L., Cousin, J., Tran, H., Amarouche, N., Engel, A., Levin, I., and Durry, G.: Temperature dependences of air-broadening, air-narrowing and line-mixing coefficients of the methane v<sub>3</sub> R6 manifold lines – application to in-situ measurements of atmospheric

Spectroscopic  
uncertainties for CH<sub>4</sub>  
from S5 and S5P

R. Checa-Garcia et al.

Title Page

Abstract

Introduction

Conclusions

References

Tables

Figures

◀

▶

◀

▶

Back

Close

Full Screen / Esc

Printer-friendly Version

Interactive Discussion



methane, J. Quant. Spectrosc. Ra., 133, 206–216, doi:10.1016/j.jqsrt.2013.08.003, 2014.  
1338

Gisi, M., Hase, F., Dohe, S., Blumenstock, T., Simon, A., and Keens, A.:  $XCO_2$ -measurements  
5 with a tabletop FTS using solar absorption spectroscopy, Atmos. Meas. Tech., 5, 2969–2980,  
doi:10.5194/amt-5-2969-2012, 2012. 1340

Guerlet, S., Butz, A., Schepers, D., Basu, S., Hasekamp, O. P., Kuze, A., Yokota, T., Blavier, J.-  
F., Deutscher, N. M., Griffith, D. W.-T., Hase, F., Kyro, E., Morino, I., Sherlock, V., Sussmann,  
R., Galli, A., and Aben, I.: Impact of aerosol and thin cirrus on retrieving and validating  $XCO_2$   
10 from GOSAT shortwave infrared measurements, J. Geophys. Res.-Atmos., 118, 4887–4905,  
doi:10.1002/jgrd.50332, 2013. 1340

Hansen, P. C.: Rank-Deficient and Discrete Ill-Posed Problems: Numerical Aspects of Linear  
Inversion, SIAM – Monographs on Mathematical Modeling and Computation 4, Philadelphia,  
USA, 1998. 1339

Hase, F., Hannigan, J., Coffey, M., Goldman, A., Höpfner, M., Jones, N., Rinsland, C.,  
15 and Wood, S.: Intercomparison of retrieval codes used for the analysis of high-  
resolution, ground-based FTIR measurements, J. Quant. Spectrosc. Ra., 87, 25–52,  
doi:10.1016/j.jqsrt.2003.12.008, 2004. 1340

Ingmann, P., Veihelmann, B., Langen, J., Lamarre, D., Stark, H., and Courrèges-Lacoste, G. B.:  
Requirements for the GMES atmosphere service and ESA's implementation concept:  
20 Sentinels-4/-5 and -5p, Remote Sens. Environ., 120, 58–69, doi:10.1016/j.rse.2012.01.023,  
2012. 1334, 1337

Kirschke, S., Bousquet, P., Ciais, P., Saunois, M., Canadell, J. G., Dlugokencky, E. J., Bergam-  
aschi, P., Bergmann, D., Blake, D. R., Bruhwiler, L., Cameron-Smith, P., Castaldi, S., Cheval-  
lier, F., Feng, L., Fraser, A., Heimann, M., Hodson, E., L., Houweling, S., Josse, B., Fraser, P.  
25 J., Krummel, P. B., Lamarque, J.-F., Langenfelds, R. L., Le Quere, C., Naik, V., O'Doherty, S.,  
Palmer, P. I., Pison, I., Plummer, D., Poulter, B., Prinn, R. G., Rigby, M., Ringeval, B., Santini,  
M., Schmidt, M., Shindell, D. T., Simpson, I. J., Spahni, R., Steele, L. P., Strode, S. A., Sudo,  
K., Szopa, S., van der Werf, G. R., Voulgarakis, A., van Weele, M., Weiss, R. F., Williams,  
J. E., and Zeng, G.: Three decades of global methane sources and sinks, Nat. Geosci., 6,  
30 813–823, 2013. 1334

Kuze, A., Suto, H., Nakajima, M., and Hamazaki, T.: Thermal and near infrared sensor  
for carbon observation Fourier-transform spectrometer on the greenhouse gases

AMTD

8, 1333–1363, 2015

Spectroscopic  
uncertainties for  $CH_4$   
from S5 and S5P

R. Checa-Garcia et al.

[Title Page](#)

[Abstract](#)

[Introduction](#)

[Conclusions](#)

[References](#)

[Tables](#)

[Figures](#)

◀

▶

◀

▶

[Back](#)

[Close](#)

[Full Screen / Esc](#)

[Printer-friendly Version](#)

[Interactive Discussion](#)



observing satellite for greenhouse gases monitoring, *Appl. Optics*, 48, 6716–6733, doi:10.1364/AO.48.006716, 2009. 1335

Meirink, J. F., Bergamaschi, P., and Krol, M. C.: Four-dimensional variational data assimilation for inverse modelling of atmospheric methane emissions: method and comparison with synthesis inversion, *Atmos. Chem. Phys.*, 8, 6341–6353, doi:10.5194/acp-8-6341-2008, 2008. 1339

Miller, C. E., Crisp, D., DeCola, P. L., Olsen, S. C., Randerson, J. T., Michalak, A. M., Alkhaled, A., Rayner, P., Jacob, D. J., Suntharalingam, P., Jones, D. B. A., Denning, A. S., Nicholls, M. E., Doney, S. C., Pawson, S., Bösch, H., Connor, B. J., Fung, I. Y., O'Brien, D., Salawitch, R. J., Sander, S. P., Sen, B., Tans, P., Toon, G. C., Wennberg, P. O., Wofsy, S. C., Yung, Y. L., and Law, R. M.: Precision requirements for space-based  $X_{CO_2}$  data, *J. Geophys. Res.*, 112, 10314, doi:10.1029/2006JD007659, 2007. 1335

Nikitin, A., Lyulin, O., Mikhailyenko, S., Perevalov, V., Filippov, N., Grigoriev, I., Morino, I., Yokota, T., Kumazawa, R., and Watanabe, T.: GOSAT-2009 methane spectral line list in the 5550–6236 cm<sup>-1</sup> range, *J. Quant. Spectrosc. Ra.*, 111, 2211–2224, doi:10.1016/j.jqsrt.2010.05.010, 2010. 1345

Nikitin, A., Boudon, V., Wenger, C., Albert, S., Brown, L., Bauerecker, S., and Quack, M.: High resolution spectroscopy and first global analysis of the Tetradecad region of methane  $^{12}CH_4$ , *Phys. Chem. Chem. Phys.*, 15, 10071–10093, doi:10.1039/C3CP50799H, 2013. 1338

O'Dell, C. W., Connor, B., Bösch, H., O'Brien, D., Frankenberg, C., Castano, R., Christi, M., Eldering, D., Fisher, B., Gunson, M., McDuffie, J., Miller, C. E., Natraj, V., Oyafuso, F., Polonsky, I., Smyth, M., Taylor, T., Toon, G. C., Wennberg, P. O., and Wunch, D.: The ACOS CO<sub>2</sub> retrieval algorithm – Part 1: Description and validation against synthetic observations, *Atmos. Meas. Tech.*, 5, 99–121, doi:10.5194/amt-5-99-2012, 2012. 1335

Oshchepkov, S., Bril, A., and Yokota, T.: PPDF-based method to account for atmospheric light scattering in observations of carbon dioxide from space, *J. Geophys. Res.*, 113, 23210, doi:10.1029/2008JD010061, 2008. 1335

Palmer, P. I., Feng, L., and Bösch, H.: Spatial resolution of tropical terrestrial CO<sub>2</sub> fluxes inferred using space-borne column CO<sub>2</sub> sampled in different earth orbits: the role of spatial error correlations, *Atmos. Meas. Tech.*, 4, 1995–2006, doi:10.5194/amt-4-1995-2011, 2011. 1335

Peters, W., Jacobson, A. R., Sweeney, C., Andrews, A. E., Conway, T. J., Masarie, K., Miller, J. B., Bruhwiler, L. M. P., Petron, G., Hirsch, A. I., Worthy, D. E. J., van der Werf, G. R., Randerson, J. T., Wennberg, P. O., Krol, M. C., and Tans, P. P.: An atmospheric perspective

## Spectroscopic uncertainties for CH<sub>4</sub> from S5 and S5P

R. Checa-Garcia et al.

[Title Page](#)

[Abstract](#)

[Introduction](#)

[Conclusions](#)

[References](#)

[Tables](#)

[Figures](#)

◀

▶

◀

▶

[Back](#)

[Close](#)

[Full Screen / Esc](#)

[Printer-friendly Version](#)

[Interactive Discussion](#)



on North American Carbon Dioxide exchange: CarbonTracker, P. Natl. Acad. Sci. USA, 104, 18925–18930, doi:10.1073/pnas.0708986104, 2007. 1338

Reuter, M., Buchwitz, M., Schneising, O., Heymann, J., Bovensmann, H., and Burrows, J. P.: A method for improved SCIAMACHY CO<sub>2</sub> retrieval in the presence of optically thin clouds, Atmos. Meas. Tech., 3, 209–232, doi:10.5194/amt-3-209-2010, 2010. 1335

5 Rodgers, C.: Inverse Methods for Atmospheric Sounding: Theory and Practice, Series on Atmospheric Oceanic and Planetary Physics, vol. 2, World Scientific Publishing Company, River Edge, NJ, USA, 2000. 1339, 1346

10 Rothman, L. S., Gordon, I. E., Babikov, Y., Barbe, A., Chris Benner, D., Bernath, P. F., Birk, M., Bizzocchi, L., Boudon, V., Brown, L. R., Campargue, A., Chance, K., Cohen, E. A., Coudert, L. H., Devi, V. M., Drouin, B. J., Fayt, A., Flaud, J.-M., Gamache, R. R., Harrison, J. J., Hartmann, J.-M., Hill, C., Hodges, J. T., Jacquemart, D., Jolly, A., Lamouroux, J., Le Roy, R. J., Li, G., Long, D. A., Lyulin, O. M., Mackie, C. J., Massie, S. T., Mikhailenko, S., Müller, H. S. P., Naumenko, O. V., Nikitin, A. V., Orphal, J., Perevalov, V., Perrin, A., Polovtseva, E. R., Richard, C., Smith, M. A. H., Starikova, E., Sung, K., Tashkun, S., Tennyson, J., Toon, G. C., Tyuterev, Vl. G., and Wagner, G.: The HITRAN 2012 molecular spectroscopic database, J. Quant. Spectrosc. Ra., 130, 4–50, doi:10.1016/j.jqsrt.2013.07.002, 2013. 1338

15 Scheepmaker, R. A., Frankenberg, C., Galli, A., Butz, A., Schrijver, H., Deutscher, N. M., Wunch, D., Warneke, T., Fally, S., and Aben, I.: Improved water vapour spectroscopy in the 4174–4300 cm<sup>-1</sup> region and its impact on SCIAMACHY HDO/H<sub>2</sub>O measurements, Atmos. Meas. Tech., 6, 879–894, doi:10.5194/amt-6-879-2013, 2013. 1346

20 Schneising, O., Buchwitz, M., Burrows, J. P., Bovensmann, H., Bergamaschi, P., and Peters, W.: Three years of greenhouse gas column-averaged dry air mole fractions retrieved from satellite – Part 2: Methane, Atmos. Chem. Phys., 9, 443–465, doi:10.5194/acp-9-443-2009, 2009. 1335

25 Schrijver, H., Gloudemans, A. M. S., Frankenberg, C., and Aben, I.: Water vapour total columns from SCIAMACHY spectra in the 2.36 μm window, Atmos. Meas. Tech., 2, 561–571, doi:10.5194/amt-2-561-2009, 2009. 1338

30 Stier, P., Feichter, J., Kinne, S., Kloster, S., Vignati, E., Wilson, J., Ganzeveld, L., Tegen, I., Werner, M., Balkanski, Y., Schulz, M., Boucher, O., Minikin, A., and Petzold, A.: The aerosol-climate model ECHAM5-HAM, Atmos. Chem. Phys., 5, 1125–1156, doi:10.5194/acp-5-1125-2005, 2005. 1339

## Spectroscopic uncertainties for CH<sub>4</sub> from S5 and S5P

R. Checa-Garcia et al.

[Title Page](#)

[Abstract](#)

[Introduction](#)

[Conclusions](#)

[References](#)

[Tables](#)

[Figures](#)

◀

▶

◀

▶

[Back](#)

[Close](#)

[Full Screen / Esc](#)

[Printer-friendly Version](#)

[Interactive Discussion](#)



- Streets, D. G., Canty, t., Carmichael, G. R., de Foy, B., Dickerson, R. R., Duncan, B. R., Edwards, D. P., Haynes, J. A., Henze, D. A., Houyoux, M. R., Jacob, D. J., Krotkov, N. A., Lamsal, L. N., Liu, Y., Lu, Z., Martin, R. V., Pfister, G. G., Pinder, R. W., Salawitch, R. J., and Wecht, K. J.: Emissions estimation from satellite retrievals: a review of current capability, *Atmos. Environ.*, 77, 1011–1042, doi:10.1016/j.atmosenv.2013.05.051, 2013. 1334
- Thompson, D. R., Benner, D. C., Brown, L. R., Crisp, D., Devi, V. M., Jiang, Y., Natraj, V., Oya fuso, F., Sung, K., Wunch, D., Castano, R., and Miller, C. E.: Atmospheric validation of high accuracy CO<sub>2</sub> absorption coefficients for the OCO-2 mission, *J. Quant. Spectrosc. Ra.*, 113, 2265–2276, doi:10.1016/j.jqsrt.2012.05.021, 2012. 1346
- Tran, H., Hartmann, J., Toon, G., Brown, L., Frankenberg, C., Warneke, T., Spietz, P., and Hase, F.: The 2v<sub>3</sub> band of CH<sub>4</sub> revisited with line mixing: consequences for spectroscopy and atmospheric retrievals at 1.67 μm, *J. Quant. Spectrosc. Ra.*, 111, 1344–1356, doi:10.1016/j.jqsrt.2010.02.015, 2010. 1338
- Tyuterev, V., Tashkun, S., Rey, M., Kochanov, R., Nikitin, A., and Delahaye, T.: Accurate spectroscopic models for methane polyads derived from a potential energy surface using high-order contact transformations, *J. Phys. Chem. A*, 117, 13779–13805, doi:10.1021/jp408116j, 2013. 1338
- Veefkind, J. P., Aben, I., McMullan, K., Förster, H., de Vries, J., Otter, G., Claas, J., Eskes, H. J., de Haan, J. F., Kleipool, Q., van Weele, M., Hasekamp, O., Hoogeveen, R., Landgraf, J., Snel, R., Tol, P., Ingmann, P., Voors, R., Kruizinga, B., Vink, R., Visser, H., and Levelt, P. F.: TROPOMI on the ESA Sentinel-5 Precursor: a GMES mission for global observations of the atmospheric composition for climate, air quality and ozone layer applications, *Remote Sens. Environ.*, 120, 70–83, doi:10.1016/j.rse.2011.09.027, 2012. 1334

[Title Page](#)[Abstract](#)[Introduction](#)[Conclusions](#)[References](#)[Tables](#)[Figures](#)[◀](#)[▶](#)[◀](#)[▶](#)[Back](#)[Close](#)[Full Screen / Esc](#)[Printer-friendly Version](#)[Interactive Discussion](#)

## Spectroscopic uncertainties for CH<sub>4</sub> from S5 and S5P

R. Checa-Garcia et al.

**Table 1.** Characteristics of simulated measurements and retrieval simulations. We investigate three retrieval configurations SW1, SW3, and SW1+3 that take into account the possible combinations of band SWIR1 and SWIR3. For each channel the signal to noise ratio (SNR) is modeled according to  $\text{SNR} = a R / \sqrt{a R + b}$  with  $R$  the backscattered radiance in units [photons s<sup>-1</sup> cm<sup>-2</sup> sr<sup>-1</sup> nm<sup>-1</sup>] and empirical parameters  $a$  and  $b$  (included on the table as SNR-a and SNR-b). The Full Width Half Maximum (FWHM) defines the width of the Gaussian instrument response function which is sampled by 2.65 pixels for each band.

Name	Used spectral range [nm]	Used spectral range [cm <sup>-1</sup> ]	Target absorbers	SW1	SW3	SW-1+3	SNR-a	SNR-b	FWHM
SWIR1	1610–1675 (divided in 2 windows)	5970–6150	CH <sub>4</sub> , CO <sub>2</sub> , H <sub>2</sub> O	✓	✓	✓	$2.132 \times 10^{-7}$	414 578	0.24 nm
SWIR3	2305–2385	4190–4340	CH <sub>4</sub> , CO	✓	✓	✓	$2.141 \times 10^{-7}$	248 836	0.24 nm

[Title Page](#)

[Abstract](#)

[Introduction](#)

[Conclusions](#)

[References](#)

[Tables](#)

[Figures](#)

◀

▶

◀

▶

[Back](#)

[Close](#)

[Full Screen / Esc](#)

[Printer-friendly Version](#)

[Interactive Discussion](#)



**Spectroscopic  
uncertainties for CH<sub>4</sub>  
from S5 and S5P**

R. Checa-Garcia et al.

**Table 2.** Experimental FTS datasets. The water vapor concentration is given as molecules cm<sup>-2</sup>. Soundings on 4 March 2013 are used as dry case and soundings on 18 June 2013 are used as humid case.

Date	Time	$\alpha_{\text{gb}}$	$X_{\text{H}_2\text{O}}$
4 Mar 2013	16:18	63°	$1.5 \times 10^{22}$
18 Jun 2013	16:37	45°	$1.07 \times 10^{23}$

- [Title Page](#)
- [Abstract](#) [Introduction](#)
- [Conclusions](#) [References](#)
- [Tables](#) [Figures](#)
- 
- [Back](#) [Close](#)
- [Full Screen / Esc](#)
- [Printer-friendly Version](#)
- [Interactive Discussion](#)



## Spectroscopic uncertainties for CH<sub>4</sub> from S5 and S5P

R. Checa-Garcia et al.

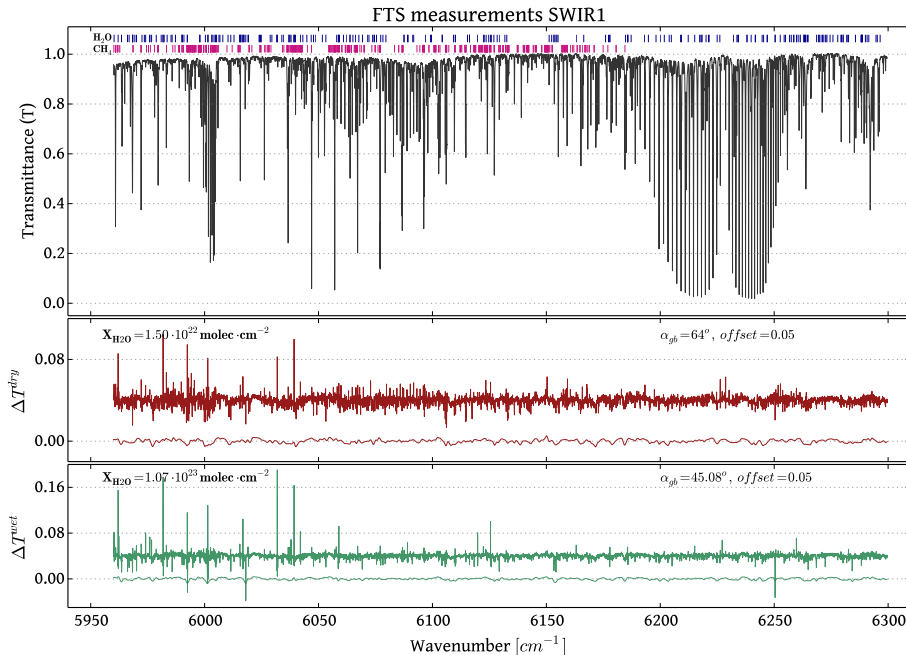


**Figure 1.** FTS transmittance spectrum in SWIR1 (upper panel) and residual transmittance for a dry day (4 March 2013) (middle panel) and a humid day (18 June 2013) (lower panel). Residual transmittance is shown at native FTS spectral resolution for dry sounding (red) and wet sounding (green) and at the typical S5 resolution of 0.24 nm with the same colors. The water vapor absorption lines (with line intensity  $\geq 10^{-26}$  [molec cm<sup>-2</sup>]) are shown with blue vertical stacks. The methane absorption lines (with line intensity  $\geq 10^{-23}$  [molec cm<sup>-2</sup>]) are shown with magenta vertical stacks.

## Spectroscopic uncertainties for CH<sub>4</sub> from S5 and S5P

R. Checa-Garcia et al.

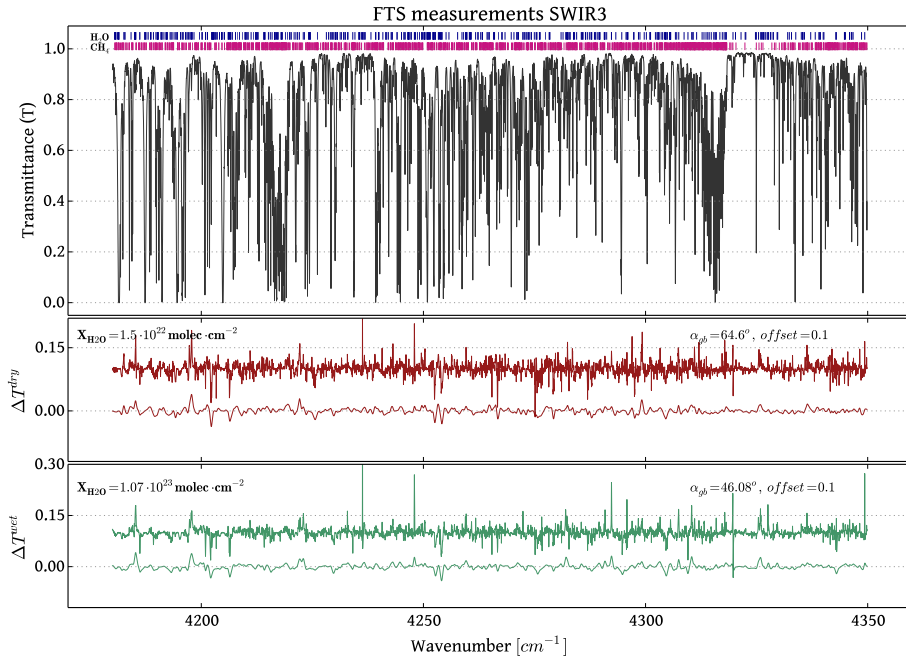


**Figure 2.** FTS transmittance spectrum in SWIR3 (upper panel) and residual transmittance for a dry day (4 March 2013) (middle panel) and a humid day (18 June 2013) (lower panel). Residual transmittance is shown at native FTS spectral resolution for dry sounding (red) and wet sounding (green) and at the typical S5 resolution of 0.24 nm with the same colors. The water vapor absorption lines (with line intensity  $\geq 10^{-26} [\text{cm}^{-1} \text{ molec}^{-1} \text{ cm}^{-2}]$ ) are shown with blue vertical stacks. The methane absorption lines (with line intensity  $\geq 10^{-23} [\text{cm}^{-1} \text{ molec}^{-1} \text{ cm}^{-2}]$ ) are shown with magenta vertical stacks.

**Spectroscopic  
uncertainties for CH<sub>4</sub>  
from S5 and S5P**

R. Checa-Garcia et al.

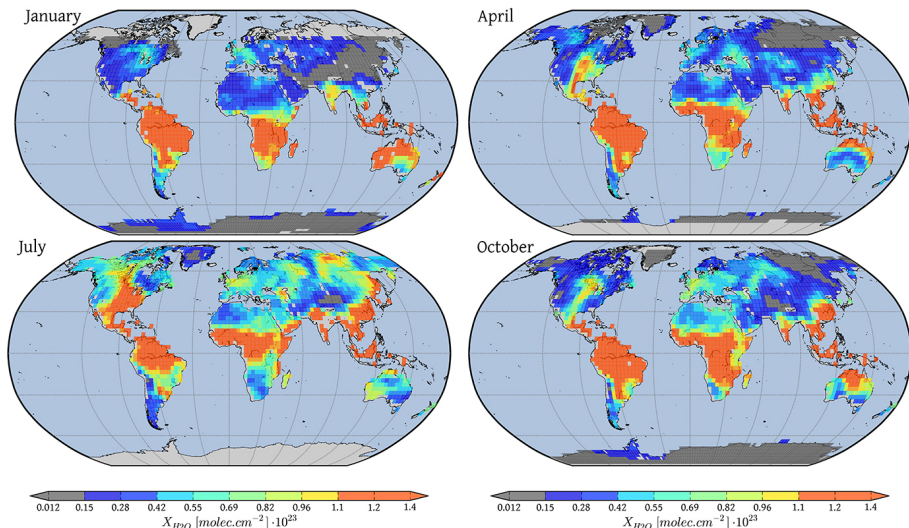


**Figure 3.** Seasonal  $XH_2O$  concentrations ( $\text{molecules cm}^{-2}$ ). Latitudes with Solar Zenith Angles larger than  $70^\circ$  were filtered.

[Title Page](#)[Abstract](#)[Introduction](#)[Conclusions](#)[References](#)[Tables](#)[Figures](#)[|◀](#)[▶|](#)[◀](#)[▶](#)[Back](#)[Close](#)[Full Screen / Esc](#)[Printer-friendly Version](#)[Interactive Discussion](#)

**Spectroscopic  
uncertainties for CH<sub>4</sub>  
from S5 and S5P**

R. Checa-Garcia et al.

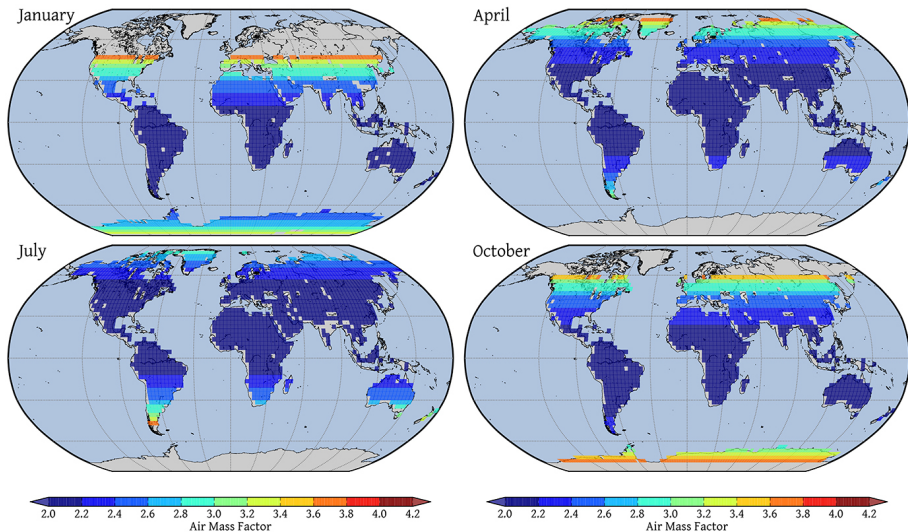


**Figure 4.** Airmass Factor (AMF) for the four seasons considered. Latitudes with Solar Zenith Angles larger than 70° were filtered.

[Title Page](#)[Abstract](#)[Introduction](#)[Conclusions](#)[References](#)[Tables](#)[Figures](#)[Back](#)[Close](#)[Full Screen / Esc](#)[Printer-friendly Version](#)[Interactive Discussion](#)

**Spectroscopic  
uncertainties for CH<sub>4</sub>  
from S5 and S5P**

R. Checa-Garcia et al.

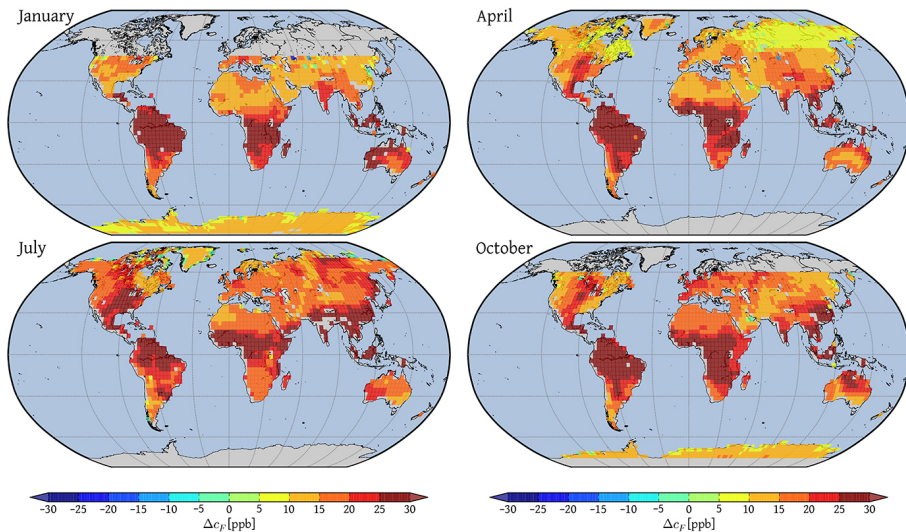


**Figure 5.** XCH<sub>4</sub> retrieval error  $\Delta c_F$  [ppb] for retrieval concept SW1 (only SWIR1 band).

[Title Page](#)[Abstract](#)[Introduction](#)[Conclusions](#)[References](#)[Tables](#)[Figures](#)[|◀](#)[▶|](#)[◀](#)[▶](#)[Back](#)[Close](#)[Full Screen / Esc](#)[Printer-friendly Version](#)[Interactive Discussion](#)

**Spectroscopic  
uncertainties for CH<sub>4</sub>  
from S5 and S5P**

R. Checa-Garcia et al.

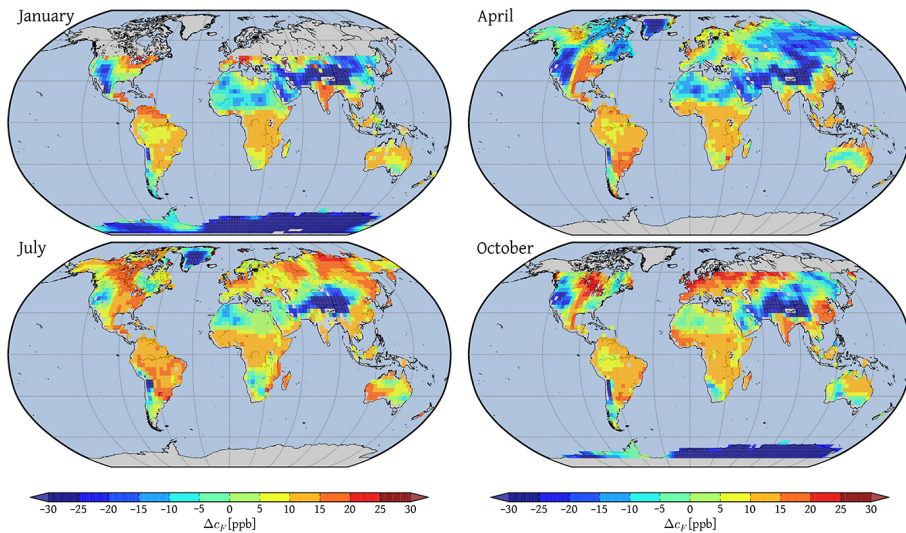


**Figure 6.** XCH<sub>4</sub> retrieval error  $\Delta c_F$  [ppb] for retrieval concept SW3 (only SWIR3 band).

[Title Page](#)[Abstract](#)[Introduction](#)[Conclusions](#)[References](#)[Tables](#)[Figures](#)[|◀](#)[▶|](#)[◀](#)[▶](#)[Back](#)[Close](#)[Full Screen / Esc](#)[Printer-friendly Version](#)[Interactive Discussion](#)

**Spectroscopic  
uncertainties for CH<sub>4</sub>  
from S5 and S5P**

R. Checa-Garcia et al.

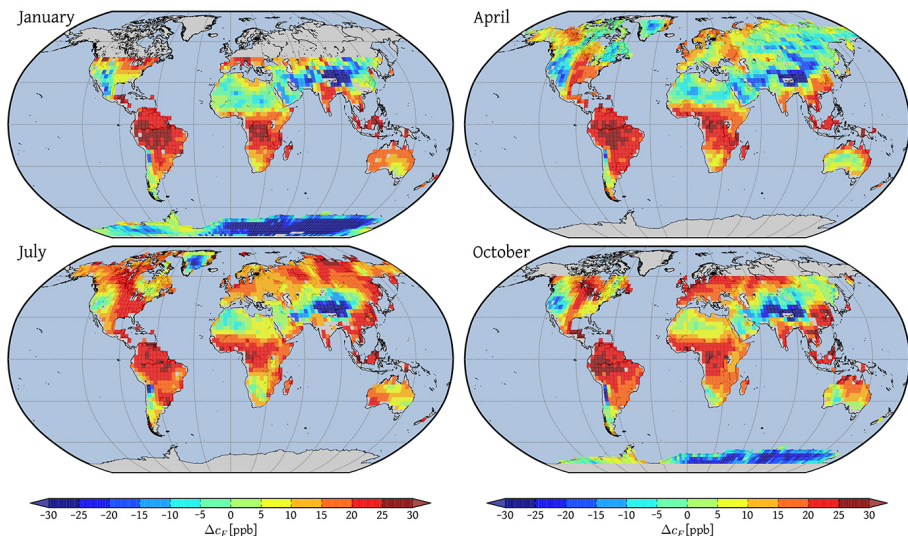


**Figure 7.** XCH<sub>4</sub> retrieval error  $\Delta c_F$  [ppb] for retrieval concept SW1+3 (both, SWIR1 and SWIR3 band).

[Title Page](#)[Abstract](#)[Introduction](#)[Conclusions](#)[References](#)[Tables](#)[Figures](#)[|◀](#)[▶|](#)[◀](#)[▶](#)[Back](#)[Close](#)[Full Screen / Esc](#)[Printer-friendly Version](#)[Interactive Discussion](#)

**Spectroscopic  
uncertainties for CH<sub>4</sub>  
from S5 and S5P**

R. Checa-Garcia et al.

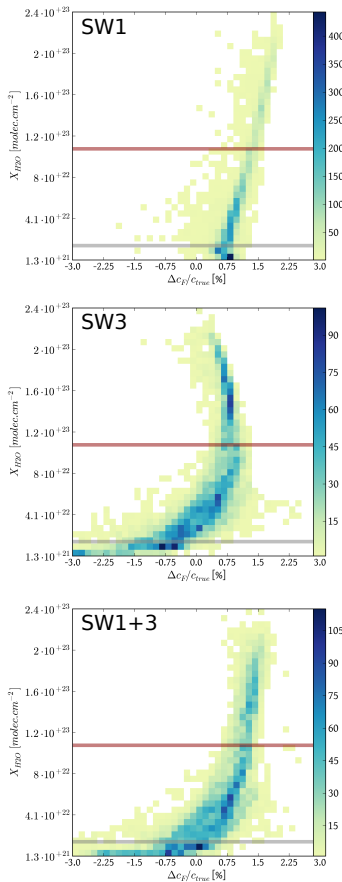


**Figure 8.** Bidimensional histograms of methane retrieval error (%) with respect to XH<sub>2</sub>O total concentration values. Spurious cases of SW-3 with very low total water vapor concentration with XCH<sub>4</sub> retrieval error smaller than −3 % located on Antarctica were excluded.